

# PACGNet: Pyramidal Adaptive Cross-Gating for Multimodal Detection

Zidong Gu , Shoufu Tian\*

*School of Mathematics, China University of Mining and Technology, Xuzhou 221116, China*

---

## Abstract

Object detection in aerial imagery is a critical task in applications such as UAV reconnaissance. Although existing methods have extensively explored feature interaction between different modalities, they commonly rely on simple fusion strategies for feature aggregation. This introduces two critical flaws: it is prone to cross-modal noise and disrupts the hierarchical structure of the feature pyramid, thereby impairing the fine-grained detection of small objects. To address this challenge, we propose the Pyramidal Adaptive Cross-Gating Network (PACGNet), an architecture designed to perform deep fusion within the backbone. To this end, we design two core components: the Symmetrical Cross-Gating (SCG) module and the Pyramidal Feature-aware Multimodal Gating (PFMG) module. The SCG module employs a bidirectional, symmetrical "horizontal" gating mechanism to selectively absorb complementary information, suppress noise, and preserve the semantic integrity of each modality. The PFMG module reconstructs the feature hierarchy via a progressive hierarchical gating mechanism. This leverages the detailed features from a preceding, higher-resolution level to guide the fusion at the current, lower-resolution level, effectively preserving fine-grained details as features propagate. Through evaluations conducted on the DroneVehicle and VEDAI datasets, our PACGNet sets a new state-of-the-art benchmark, with mAP50 scores reaching 81.7% and 82.1% respectively.

Keywords: Multimodal Object Detection, RGB-Infrared Fusion, Aerial Imagery, Cross-Modality Interaction, Gating Mechanisms.

---

## 1. Introduction

Object detection, a cornerstone of computer vision, is pivotal in applications like autonomous driving[1] and unmanned aerial vehicle (UAV)[2] reconnaissance. However, object detection in aerial imagery is confronted with difficulties, such as the prevalence of small-scale objects[3], complex backgrounds, and inconsistent lighting[4]. Consequently, RGB-based object detection[5] suffers from drastic performance degradation under adverse conditions such as low light or strong glare. Concurrently, single-modality detection using only infrared (IR) images[6], while robust to lighting, often lack the rich texture and fine-grained class details present in RGB imagery. This inherent bottleneck in single-modality perception makes the fusion of RGB and IR data an essential pathway toward achieving robust, all-weather, and all-scenario object detection[7][8][9].

Despite its promise, existing dual-modality methods face critical challenges. Current dual-modality fusion methods are mainly divided into pixel-level[10][11], feature-level[12][13][14], and decision-level[15] fusion, with feature-level fusion methods being superior to pixel-level and decision-level fusion methods[16][17]. In feature-level fusion, many approaches employ a dual-stream backbone for feature extraction, followed by information interaction and simple additive fusion at different levels of the feature pyramid (e.g., P2, P3, P4, P5)[7][18]. This common paradigm, however, introduces two fundamental problems. First, it leads to noise introduction and a loss of interpretability. Naive feature interaction can cause one modality to be contaminated by noise from the other[12][19] (e.g., invalid features from an overexposed RGB image), complicating subsequent representation learning. More critically, once interacted, the features in the RGB and IR branches no longer retain their clear, single-modality semantics, which undermines the interpretability and controllability of each branch. Second, this approach results in a weakened feature hierarchy and an over-reliance on the neck network. By performing simple, layer-wise addition,

\* Corresponding author.

E-mail address: shoufu2006@126.com.

the crucial task of deep fusion is effectively offloaded to the detection neck (e.g., PAN)[20]. This dilutes the inherent hierarchical relationships within the backbone's feature pyramid, leaving the features fed into the neck too disconnected to support the cross-level collaboration between detail and semantics that is vital for detecting small objects.

To resolve these issues, this paper introduces the Pyramidal Adaptive Cross-Gating Network (PACGNet), an architecture designed to perform true multimodal fusion before the neck through two novel mechanisms: "horizontal guidance" and "vertical refinement." To counteract noise and maintain interpretability, we propose the Symmetrical Cross-Gating (SCG) module. Inserted at multiple scales within the backbone, SCG employs a bidirectional, symmetrical gating mechanism across both spatial and channel dimensions. This allows it to selectively introduce complementary information from the opposing modality while suppressing noise and, via a residual connection, preserving the stable semantic integrity of the original modality. To address the weakened hierarchy, we present the Pyramidal Feature-aware Multimodal Gating (PFMG) module. Positioned before the neck, PFMG rebuilds hierarchical connections by using the fused feature from the preceding, higher-resolution level as a spatial context prior. This prior gates the fusion process at the current level, ensuring a detail-aware fusion cascade down the feature pyramid. This approach internalizes deep fusion and hierarchical modeling within the backbone, producing a single-stream, fused feature pyramid that is readily compatible with standard detection necks and heads.

In summary, the contributions of this paper are as follows:

1. We propose the novel PACGNet framework, which completes deep fusion within the backbone to generate a single feature pyramid seamlessly compatible with any standard detection neck.
2. We design the Symmetrical Cross-Gating (SCG) module to enable adaptive "horizontal" feature interaction, which selectively fuses complementary information while suppressing cross-modal noise.
3. We develop the Pyramidal Feature-aware Multimodal Gating (PFMG) module, which rebuilds the feature hierarchy via a top-down gating mechanism to preserve the fine-grained details crucial for small object detection.
4. The effectiveness and superiority of the proposed method are demonstrated on two challenging UAV-based multimodal detection benchmarks, DroneVehicle and VEDAI, achieving state-of-the-art performance with mA P50 scores of 81.7% and 82.1%, respectively.

The organization of the remaining sections of this paper is as follows: Section 2 reviews related work in multimodal fusion architectures, dynamic information filtering, and attention mechanisms. Section 3 provides a detailed description of our proposed PACGNet methodology, including its overall architecture, the Symmetrical Cross-Gating (SCG) module for horizontal feature interaction, and the Pyramidal Feature-aware Multimodal Gating (PFMG) module for vertical feature refinement. In Section 4, we present our experimental setup, including the datasets and evaluation metrics used, implementation details, and a comprehensive analysis of the results, along with an ablation study to validate the contributions of each component. Finally, Section 5 provides a conclusion summarizing the work and suggests directions for future research.

## 2. Related work

### 2.1. Multimodal Fusion Architectures for Object Detection

RGB-Infrared (RGB-IR) fusion significantly enhances aerial object detection performance by combining the textural richness of visible light with the stability of thermal radiation. Early research primarily focused on feature-level fusion within dual-stream backbones. Qingyun et al. [18] proposed the Cross-modality Fusion Transformer (CFT), pioneering the use of self-attention to simultaneously model intra-modal long-range dependencies and inter-modal interactions for global context-aware fusion. Zhang et al. [8] introduced SuperYOLO, integrating a super-resolution branch into the YOLO framework to augment small-target features through infrared-visible fusion. Sun et al. [21] designed UA-CMDet, incorporating an uncertainty-aware module to quantify cross-modal detection confidence and suppress the influence of low-confidence targets. Transformer-based frameworks have emerged as a dominant trend due to their global modeling capabilities: Yuan and Wei [22] developed C<sup>2</sup>Former, utilizing cross-modal attention and adaptive feature sampling for efficient feature alignment and fusion; Wang et al. [23] constructed FFODN et, which suppresses interfering features through joint expression optimization and task-specific enhancement modules. Recent studies emphasize lightweight design and hierarchical fusion: Bao et al. [12] proposed DDCINet, employing dual-dynamic cross-modal interaction to address modality inconsistency and redundancy; Liu et al. [24] designed a multi-branch progressive fusion network with a Modality Complementary Information Filter (MCIF) for adaptive fusion of modal advantages.

However, existing methods predominantly concentrate on aligning and fusing features from the same hierarchical level across modalities, overlooking two critical issues: preserving interpretability during backbone feature extraction and modeling cross-level feature relationships after fusion. Our PACGNet addresses these gaps through Symmetrical Cross-Gating (SCG) and Pyramidal Feature-aware Multimodal Gating (PFMG), achieving deep hierarchical fusion within the backbone to generate a single fused feature pyramid for input to the neck network.

## 2.2. Dynamic Complementary Information Filtering and Noise Suppression

The core challenge in cross-modal fusion lies in precisely excavating complementary information while suppressing redundant features and noise interference—a critical balance for enhancing fusion quality. Researchers have proposed several strategies:

Zhang et al. [25] proposed Guided Attentive Feature Fusion (GAFF), utilizing inter- and intra-modality attention modules to dynamically weigh and fuse multispectral features for pedestrian detection. Qingyun and Zhaokui [26] designed a Cross-Modal Attentive Feature Fusion (CMAFF) mechanism with differential enhancement and common feature selection modules. Recent approaches adopt learned alignment: Chen et al. [27] developed Offset-Aware Adaptive Feature Alignment (OAAFA) to implicitly learn optimal fusion positions; Zhao et al. [7] leveraged visible-light reflectance features in RGFNet to guide cross-modal alignment; Ouyang et al. [28] addressed pretraining modality bias via cross-modal interaction in M<sup>2</sup>FP.

While these methods advance alignment and complementary information extraction, dynamic control over complementary information filtering intensity and preservation of original semantics remains under-explored. Our Symmetrical Cross-Gating (SCG) module tackles this through a bidirectional spatial-channel gating mechanism that adaptively filters cross-modal complementary features, dynamically suppresses noise, and preserves original semantic integrity via residual connections—synergistically optimizing complementary enhancement and feature stability.

## 2.3. Attention Mechanisms for Feature Optimization

Attention mechanisms play an indispensable role in optimizing feature quality for complex scenarios by dynamically focusing on critical regions and suppressing irrelevant information, particularly for aerial imagery where targets intertwine with cluttered backgrounds. Existing studies explore attention from diverse dimensions: Woo et al.

[29] proposed the Convolutional Block Attention Module (CBAM), aggregating key features through cross-dimensional interactions. Wang et al. [30] developed ECA-Net, constructing lightweight channel attention via adaptive convolutional kernels for local cross-channel interaction.

To address the prevalence of small targets in aerial imagery—where features are easily overwhelmed by backgrounds—researchers have refined attention mechanisms: Zhang et al. [11] enhanced the Mamba architecture by integrating the Enhanced Small Target Detection (ESTD) module and Convolutional Attention Residual Gating (CAR G) module to amplify small-target feature responses. Liu et al. [24] proposed Global-Local Synergistic Attention (GLSA), which models target-background contextual relationships via global-local fusion to improve feature discriminability. Lightweight designs further facilitate practical deployment: Zhang et al. [31] proposed the GHOST framework with hybrid quantization and knowledge distillation, preserving attention efficacy while ensuring efficiency.

Building on these insights, our work adopts global-local context modeling to strengthen interactions tailored for aerial scenes. Crucially, the PFMG module leverages high-level fused features as hierarchical priors, employing a top-down gating mechanism to preserve fine-grained details essential for small object detection—thereby enhancing attention’s applicability in multimodal fusion scenarios.

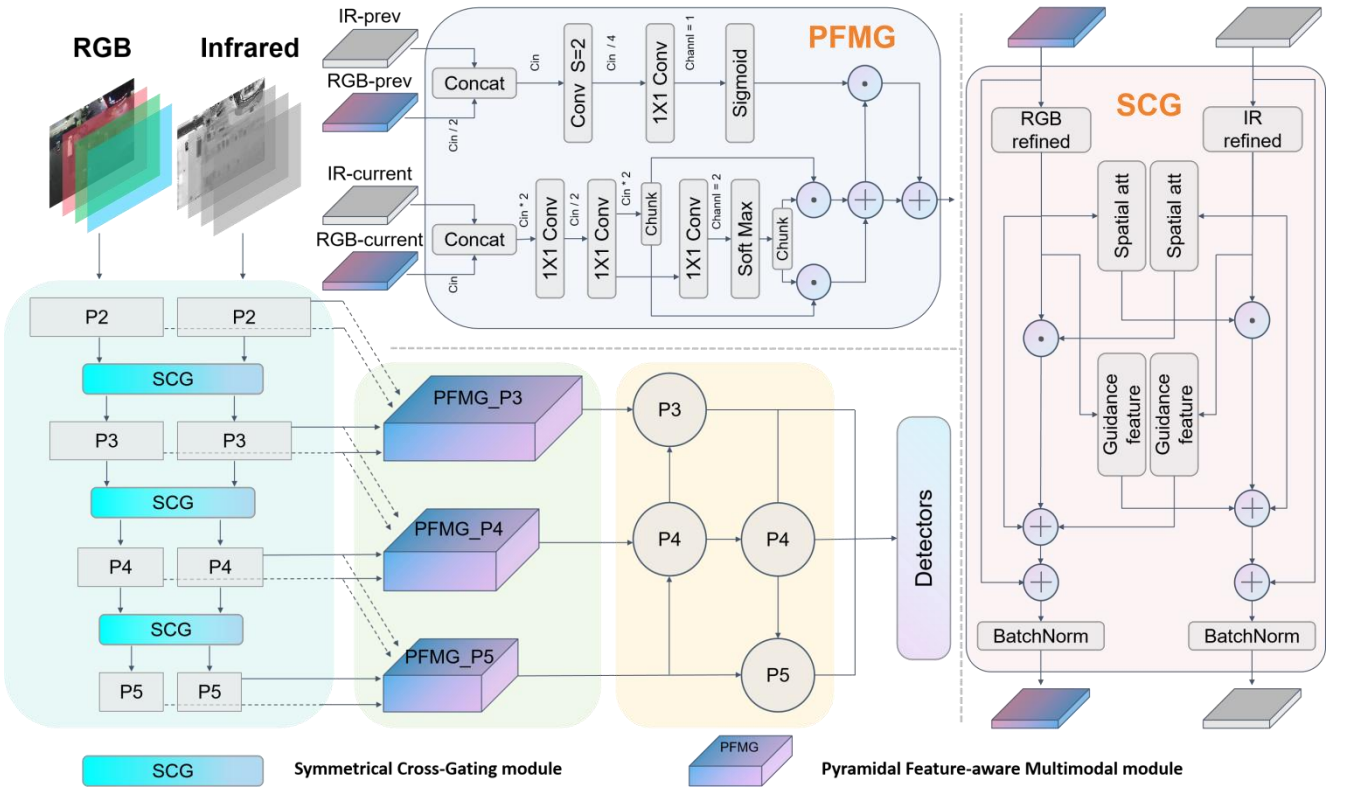


**Figure 1.** The overall framework of PACGNet. The network employs a Siamese backbone to extract RGB and infrared features in parallel, interacting via Symmetrical Cross-Gating (SCG) modules. The SCG modules are shown schematically to represent the symmetrical, bi-directional enhancement between the two modalities. Subsequently, Pyramidal Feature-aware Multimodal Gating (PFMG) modules deeply fuse the multi-scale features, which are finally processed by a Path Aggregation Network (PAN) and fed to detectors for prediction.

### 3. Methodology

In this section, we present the detailed architecture of our proposed Pyramidal Adaptive Cross-Gating Network (PACGNet). As established in the introduction, PACGNet is built upon the core principles of "horizontal" interaction and "vertical" refinement. We begin with an overview of the overall framework, followed by a detailed exposition of our two core contributions: the Symmetrical Cross-Gating (SCG) module, which materializes the horizontal, intra-scale feature synergy, and the Pyramidal Feature-aware Multimodal Gating (PFMG) module, which accomplishes the vertical, top-down feature fusion. Finally, we clarify the loss function employed for model optimization.

### 3.1. Overall Architecture

The architecture of PACGNet is built upon a dual-stream backbone derived from YOLOv8[32], meticulously designed to process RGB and infrared (IR) images in parallel. Notably, the RGB and IR branches share identical network topology but maintain completely independent trainable weights, with all parameters initialized randomly (no pre-trained weights from external datasets are used). The overall framework of the network is illustrated in Figure 1. Each stream independently extracts multi-scale features from its respective modality. The core innovation of our work lies in the strategic integration of the proposed SCG and PFMG modules to create a deeply fused and context-aware feature hierarchy.

The data flow is as follows:

**3.1.1. Dual-Stream Backbone:** The network begins with two parallel branches, each processing one modality (RGB or IR). Each branch consists of standard convolutional layers and C2f blocks to extract features at progressively coarser resolutions.

**3.1.2. Inter-Modal Fusion with SCG:** Symmetrical Cross-Gating (SCG) modules are inserted into the backbone after the P2, P3, and P4 feature stages. At each stage, the SCG module (Figure 1) takes feature maps from both the RGB and IR streams and performs a bi-directional enhancement, allowing for a mutual exchange of information. This process ensures a deep and continuous interaction between modalities throughout feature extraction.

**3.1.3. Intra-Backbone Hierarchical Refinement with PFMG:** After the dual-stream backbone has extracted a full pyramid of features, but before these features enter the neck, we introduce the Pyramidal Feature-aware Multimodal Gating (PFMG) modules. The detailed structure of the PFMG module is also illustrated within the overall framework in Figure 1, and it performs a top-down fusion and refinement within the backbone itself. Specifically, the fused features from a higher-resolution, finer-grained level are used to gate the fusion of the two modalities at the current, lower-resolution level (e.g., P3 features guide the fusion of P4 features). This synergistic process merges the dual-stream features into a single, powerful, context-aware fused feature map at each level (P\_fused\_3, P\_fused\_4, P\_fused\_5).

**3.1.4. Detection Head:** These highly-refined fused feature maps are subsequently passed to a standard YOLO v8 neck and detection head for final oriented object detection.

### 3.2. Symmetrical Cross-Gating (SCG) Module

Before the final fusion, effectively exchanging information and enhancing features between the RGB and IR streams is a fundamental challenge. A naive approach can propagate redundant or noisy information, degrading feature quality. To address this, we propose the Symmetrical Cross-Gating (SCG) module, designed to facilitate a sophisticated, bi-directional feature enhancement and interaction that adaptively highlights complementary cues while a

ctively suppressing redundancy. While Figure 1 illustrates the schematic placement of SCG modules within the overall architecture, the detailed internal architecture of this module is depicted in Figure 2. The process for the RG B feature path, guided by the IR path, is detailed below (a symmetrical process occurs for the IR path).

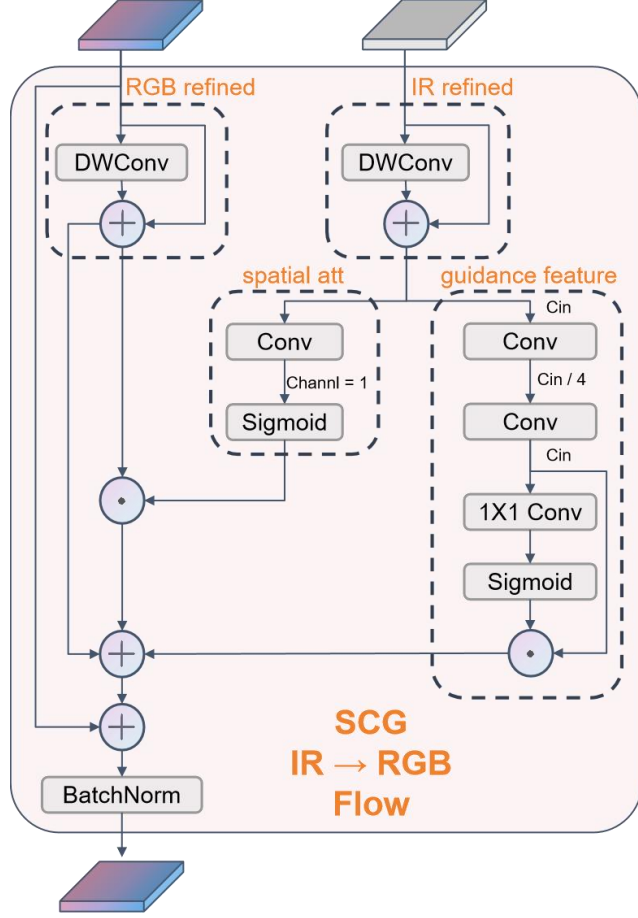


**Figure 2.** Detailed architecture of the Symmetrical Cross-Gating (SCG) module. Illustrating the IR-to-RGB guidance path, with its symmetrical counterpart omitted for brevity. The module utilizes a refined IR feature to generate parallel spatial and channel-wise guidance. This guidance modulates and enhances the refined RGB feature, with a final residual connection preserving the original information.

**Step 1: Intra-Modal Feature Refinement:** Each input feature map,  $F_{rgb}^{in}$  and  $F_{ir}^{in}$ , first passes through a Refined Feature Extractor. This extractor, composed of efficient Depthwise Separable Bottleneck blocks, enhances its intra-modal representation:

$$F'_{rgb} = R(F_{rgb}^{in})$$

$$F'_{ir} = R(F_{ir}^{in}) \quad (1)$$

where  $R(\bullet)$  denotes the Refined Feature Extractor.

**Step 2: Cross-Modal Spatial Guidance:** A spatial attention map  $M_S^{ir \rightarrow rgb}$  is generated from the refined IR features to spatially modulate the refined RGB features. This map is generated by a 1x1 convolution followed by

a Sigmoid function. The modulation uses a  $(1 + M)$  scheme to ensure a residual connection, preventing information loss if the gate is zero.

$$\begin{aligned} M_S^{ir \rightarrow rgb} &= \sigma(\text{Conv}_{1 \times 1}(F'_{ir})) \\ \tilde{F}_{rgb} &= F'_{rgb} \odot (1 + M_S^{ir \rightarrow rgb}) \end{aligned} \quad (2)$$

where  $\sigma$  is the Sigmoid function and  $\odot$  denotes element-wise multiplication.

**Step 3: Gated Cross-Modal Feature Guidance:** Concurrently, refined IR features are projected into a guidance feature map  $G_{rgb}$  via a projection block  $P_{ir \rightarrow rgb}(\bullet)$ , which uses a bottleneck design for efficiency. An adaptive channel-wise gate  $g_{rgb}$  is generated from this guidance feature to control its contribution. This gating mechanism is crucial for suppressing redundancy, as it learns to down-weight guidance from a noisy or uninformative modality.

$$\begin{aligned} G_{rgb} &= P_{ir \rightarrow rgb}(F'_{ir}) \\ g_{rgb} &= \sigma(\text{Conv}_{1 \times 1}(G_{rgb})) \end{aligned} \quad (3)$$

**Step 4: Final Fusion:** The spatially guided features and the gated feature guidance are combined and added back to the original input feature via a residual connection. This preserves the original feature flow and ensures stable training.

$$F_{rgb}^{out} = \text{Norm}(F_{rgb}^{in} + (\tilde{F}_{rgb} + g_{rgb} \odot G_{rgb})) \quad (4)$$

### 3.3. Pyramidal Feature-aware Multimodal Gating (PFMG) Module

A key design choice in PACGNet is to finalize multimodal fusion before the neck network. This approach produces a single, powerful feature pyramid (P\_fused\_3, P\_fused\_4, P\_fused\_5), ensuring maximum modularity and seamless compatibility with any standard detection neck and head designed for single-modality inputs. By generating a refined, single-stream feature pyramid, our fusion backbone can seamlessly interface with any standard, advanced detection neck and head (such as the PANet in YOLOv8) designed for single-modality inputs. This strategy obviates the need for complex modifications to the subsequent detection pipeline and enhances the model's extensibility.

A primary challenge in deep backbones is the progressive loss of spatial detail due to repeated downsampling. To mitigate this, the PFMG module introduces a progressive, hierarchically-aware fusion strategy.

The design synergizes with the natural forward information flow of the backbone network, where features at level  $P_i$  are generated from level  $P(i-1)$ . Our core idea is to leverage the feature map from the preceding level  $P(i-1)$ —which contains the richest spatial details right before they are downsampled—as an explicit guidance signal for the fusion process at the current level  $P_i$ . This creates a cascade where the fusion at each level is conditioned on the high-fidelity spatial context of the previous level, ensuring that crucial details for small objects are actively

preserved throughout the feature pyramid. The process to generate the refined feature  $F_{\text{fused}}^{(i)}$  for level  $i$  is as follows:

**Step 1: Hierarchical Spatial Gate:** The module takes features from the current level  $(F_{\text{rgb}}^{(i)}, F_{\text{ir}}^{(i)})$  and the previous, higher-resolution level  $(F_{\text{rgb}}^{(i-1)}, F_{\text{ir}}^{(i-1)})$  as input. The previous-level features are concatenated and passed through a Hierarchical Spatial Gate, which uses a strided convolution (stride=2). This single operation efficiently downsamples the features and generates a spatial gate  $M_S^{(i)}$  that encodes rich, fine-grained contextual cues at the current level's resolution.

$$M_S^{(i)} = H(\text{Concat}(F_{\text{rgb}}^{(i-1)}, F_{\text{ir}}^{(i-1)})) \quad (5)$$

Where  $H(\bullet)$  denotes the Hierarchical Spatial Gate.

**Step 2: Modality Interaction and Adaptive Weighting:** The current-level features are concatenated and passed through a modality\_interaction block (a bottleneck of 1x1 convolutions) to produce interacted features, which are then split back into RGB and IR streams,  $F'_{\text{rgb}}$  and  $F'_{\text{ir}}$ . These are then used to compute adaptive, pixel-wise fusion weights via a 1x1 convolution followed by a Softmax function, ensuring the weights  $(\omega_{\text{rgb}}^{(i)}, \omega_{\text{ir}}^{(i)})$  sum to one at each spatial location.

$$\begin{aligned} [F'_{\text{rgb}}, F'_{\text{ir}}] &= \text{Split}(I(\text{Concat}(F_{\text{rgb}}^{(i)}, F_{\text{ir}}^{(i)}))) \\ [\omega_{\text{rgb}}^{(i)}, \omega_{\text{ir}}^{(i)}] &= \text{Softmax}(\text{Conv}_{1 \times 1}(\text{Concat}(F'_{\text{rgb}}, F'_{\text{ir}}))) \end{aligned} \quad (6)$$

**Step 3: Hierarchically Gated Fusion:** The fusion is a two-step process. First, a base fused feature is computed via a weighted average of the interacted features. Second, this representation is additively modulated by the hierarchical spatial gate from Step 1.

$$\begin{aligned} F_{\text{base}}^{(i)} &= \omega_{\text{rgb}}^{(i)} \odot F'_{\text{rgb}} + \omega_{\text{ir}}^{(i)} \odot F'_{\text{ir}} \\ F_{\text{fused}}^{(i)} &= F_{\text{base}}^{(i)} + M_S^{(i)} \odot F_{\text{base}}^{(i)} \end{aligned} \quad (7)$$

### 3.4. Loss Function

For bounding box regression, a crucial component of object detection, we employ the Wise-IoU (WIoU) v3[33] loss function. Unlike traditional IoU-based losses, WIoU introduces a dynamic, non-monotonic focusing mechanism that intelligently assigns smaller loss weights to easy, high-quality examples and larger weights to difficult, low-quality anchor boxes. This allows the model to focus its learning capacity on challenging examples during training, improving the overall robustness and localization accuracy of the detector. To ensure a fair and rigorous comparison, all experiments presented in this paper, including our baseline and all ablation models, were trained using the WIoU loss function.

## 4. Experiments

This section elaborates on the experimental configuration, including the datasets employed and evaluation metrics. Subsequently, we present a comprehensive quantitative analysis, encompassing comparative assessments against relevant detectors, ablation studies investigating component contributions, and evaluations of model generalizability. Visualized results are also provided to offer intuitive insights into our findings.

### 4.1. Datasets and Evaluation Metrics

**DroneVehicle.** Our experiments primarily utilized the DroneVehicle dataset[34]. This is a public benchmark for UAV visible-infrared object detection, comprising 28,439 registered RGB-infrared image pairs from diverse diurnal/nocturnal scenarios (e.g., urban roadways, residential sectors) with five vehicle categories. This dataset uses annotations with oriented (rotated) bounding boxes (OBB). Original  $840 \times 712$  images were preprocessed by removing borders to yield  $640 \times 512$  effective regions, then resized to  $640 \times 640$  for input. We adhered to the standard split (17,990 training, 1,469 validation, 8,980 testing pairs), with infrared annotations exclusively serving as ground truth.

**VEDAI.** Furthermore, we extended our evaluations to the VEDAI dataset[35]. This is a multispectral aerial imagery benchmark for vehicle detection. It consists of 1,210 strictly registered image pairs with a resolution of  $1024 \times 1024$ , encompassing nine object categories. The VEDAI dataset features annotations with oriented (rotated) bounding boxes (OBB) and is characterized by a preponderance of small objects, posing a significant challenge for detectors.

**Evaluation Metrics.** For overall performance comparison, we adopt mean Average Precision at an IoU threshold of 0.5 (mAP50) as our primary evaluation metric. Additionally, we provide per-category AP50 scores to facilitate a finer-grained analysis of the model's performance on specific object classes. Specifically, mAP50 denotes the mean Average Precision calculated across all object categories at a fixed IoU threshold of 0.50, which determines true positives (TPs) and false positives (FPs), as we aim to focus on the most widely used benchmark in related multispectral object detection research.

### 4.2. Implementation Details

The proposed PACGNet model was implemented using the Ultralytics YOLOv8 v8.2.50 framework[32]. All experiments were executed on a server equipped with 8 NVIDIA GeForce RTX 3090 GPUs (24GB VRAM each), operating within a Python 3.10.15 environment. The model architecture builds upon the standard YOLOv8 dual-stream backbone, integrating our proposed PFMG (Pyramidal Feature-aware Multimodal Gating) and SCG (Symmetrical Cross-Gating) modules to effectively enhance cross-modal feature interaction and adaptive fusion.

Model optimization was performed using the Stochastic Gradient Descent (SGD) optimizer with a batch size of 128 and 4 parallel data loading workers per GPU. Key hyperparameters included an initial learning rate (lr0) of 0.01, a final learning rate factor (lrf) of 0.01, momentum set to 0.937, and weight decay configured to 0.0005. A learning rate warmup schedule spanning 3.0 epochs was employed, featuring an initial momentum of 0.8 and an initial bias learning rate of 0.1. Training was conducted for a maximum of 300 epochs. Data augmentation strategies included Mosaic image composition, random horizontal and vertical flipping, and random translation.

### 4.3. Results Analysis

**Table 1.** Comparative performance analysis of the proposed PACGNet against SOTA single and multi-modality object detectors on the DroneVehicle test dataset. Metrics include per-category Average Precision (AP50) and overall mean Average Precision (mAP50) at IoU=0.5. Best results are highlighted in red; second-best results are underlined.

Detectors	Visible	Infrared	car	truck	bus	van	freight	car	mAP50
S <sup>2</sup> A-Net[36]	✓		79.9	50.0	82.8	37.5	36.2		57.3
Oriented R-CNN[19]	✓		80.1	53.8	85.4	43.3	41.6		60.8
RoI Transformer[37]	✓		61.6	55.1	85.5	44.8	42.3		61.6
YOLOv8n[32]	✓		96.2	72.7	94.5	54.4	53.2		74.2
S <sup>2</sup> A-Net[36]		✓	89.7	51.0	89.0	44.0	50.2		64.8
Oriented R-CNN[19]		✓	89.8	57.4	89.3	45.4	53.1		67.0
RoI Transformer[37]		✓	90.1	60.4	89.7	52.2	58.9		70.3
YOLOv8n[32]		✓	97.7	75.5	94.7	57.6	61.2		77.4
UA-CMDet[21]	✓	✓	87.5	60.7	87.1	38.0	46.8		64.0
LF-MDet[38]	✓	✓	82.2	73.6	86.6	57.0	59.6		71.8
C <sup>2</sup> Former[22]	✓	✓	90.2	68.3	89.8	58.5	64.4		74.2
CALNet[39]	✓	✓	90.3	76.2	89.1	58.5	63.0		75.4
DDCINet[12]	✓	✓	91.0	78.9	90.7	65.5	66.1		78.4
M2FP[28]	✓	✓	95.7	76.2	92.1	64.7	64.7		78.7
OAFA[27]	✓	✓	90.3	76.8	90.3	<b>66.0</b>	<b>73.3</b>		79.4
MGMF[40]	✓	✓	91.4	70.1	91.1	<b>69.4</b>	<b>78.5</b>		80.3
RGFNet[7]	✓	✓	<b>98.4</b>	<b>81.1</b>	<b>95.8</b>	63.0	68.7	<b>81.4</b>	
PACGNet(our)	✓	✓	<b>98.4</b>	<b>81.8</b>	<b>96.2</b>	63.1	69.2	<b>81.7</b>	

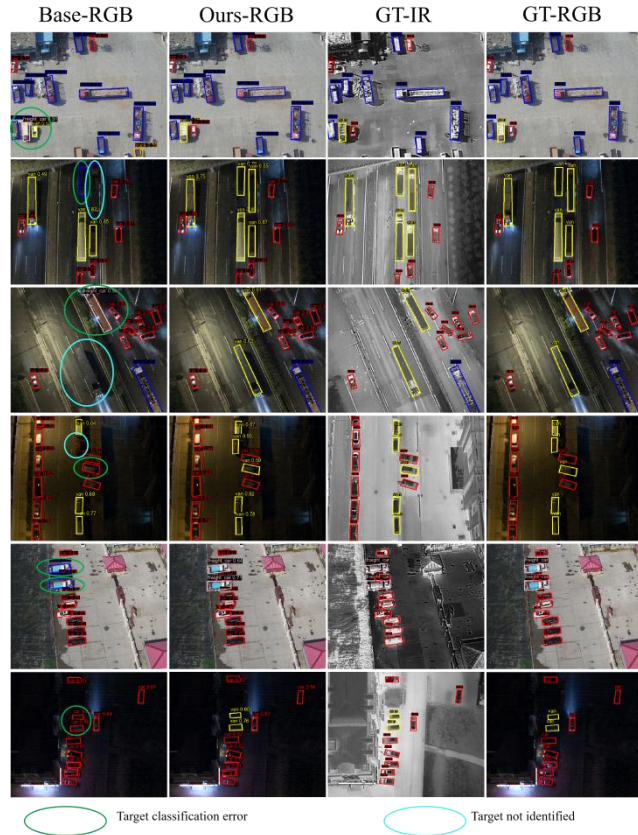


**Figure 3.** Visualization of the qualitative comparison between the baseline model and our improved PACGNet, alongside the ground truth, under various lighting conditions in the DroneVehicle dataset. The four columns, from left to right, display: the detection results of the Baseline model, the detection results of the improved PACGNet, the ground truth of the infrared image (GT-IR), and the ground truth of the visible light image (GT-RGB). The six rows illustrate six different lighting scenarios.

#### 4.3.1 Performance on the DroneVehicle Dataset:

We evaluated PACGNet on the DroneVehicle test dataset, with quantitative results presented in Table 1. Our model achieves a state-of-the-art 81.7% mAP50, marking a 4.3% absolute improvement over the best single-modality detector (YOLOv8n, 77.4% mAP50). These results clearly demonstrate the significant performance gains from our multi-modal fusion strategy compared to approaches relying on a single spectrum.

Positioned against contemporary state-of-the-art (SOTA) multi-modality detectors, PACGNet demonstrated exceptional competitiveness, establishing a new benchmark with a leading mAP50 score of 81.7%. This result comprehensively surpasses all other compared models, including the second-best method RGFNet (81.4% mAP50) by 0.3%. Furthermore, PACGNet established clear advantages over other strong contenders, exceeding MGMF (80.3%), OAFA (79.4%), M2FP (78.7%), and DDCINet (78.4%) by 1.4%, 2.3%, 3.0%, and 3.3% in mAP50, respectively, thereby validating the advanced nature of our design.

A finer-grained analysis at the category level reveals PACGNet's specific strengths and challenges. The model exhibits outstanding performance for key classes, achieving an exceptionally high 98.4% AP50 for 'car' detection (tying with RGFNet) and securing the top scores among all compared methods for both 'bus' (96.2% AP50) and 'truck' (81.8% AP50), highlighting the effectiveness of our PFMG and SCG modules. Conversely, for the visually ambiguous 'van' (63.1% AP50) and 'freight car' (69.2% AP50) categories – where aerial views often present similarities ('van' to 'car', 'freight car' to 'truck') – PACGNet's accuracy, while competitive, remains lower than that achieved by methods such as OAFA and MGMF. We attribute this performance difference partly to architectural choices; our efficient single-stage approach prioritizes speed, whereas the two-stage architectures often employed by methods like OAFA and MGMF may possess superior capabilities for the fine-grained feature discrimination crucial for distinguishing these challenging, visually similar classes. To provide a more intuitive validation of our model's superiority, Figure 3 presents a qualitative comparison of detection results from the baseline and PACGNet under various lighting conditions.

**Table 2.** Comparative performance analysis of the proposed PACGNet against SOTA methods on the VEDAI dataset. The evaluation is for oriented bounding box (OBB) detection. Metrics include per-category Average Precision (AP) and overall mean Average Precision (mAP). Best results are highlighted in red; second-best results are underlined.

Detectors	Visible	Infrared	car	truck	tractor	camping_car	van	vehicle	pickup	boat	mAP50
YOLOv8n	✓		89.4	80.6	76.6	79.0	<b>83.0</b>	60.4	84.9	52.2	75.8
YOLOv8n		✓	84.5	81.4	46.9	80.2	<b>83.9</b>	42.6	84.9	56.3	70.1
YOLOFusion[41]	✓	✓	<b>91.7</b>	78.1	71.9	78.9	75.2	54.7	85.9	71.7	75.9
OST[31]	✓	✓	91.1	<b>82.2</b>	84.9	74.9	82.9	64.6	<b>87.7</b>	60.2	78.6
SuperYOLO[8]	✓	✓	91.1	70.2	80.4	79.3	76.5	57.3	85.7	60.2	76.5
ICAFusion[42]	✓	✓	-	-	-	-	-	-	-	-	76.6
$S_4^6$ -MSTD[11]	✓	✓	<b>91.8</b>	78.5	<b>85.8</b>	<b>82.3</b>	81.6	<b>84.6</b>	69.3	<b>75.6</b>	<b>81.2</b>
PACGNet(our)	✓	✓	90.5	<b>87.1</b>	<b>87.4</b>	<b>80.8</b>	82.5	<b>64.6</b>	<b>87.4</b>	<b>76.8</b>	<b>82.1</b>

#### 4.3.2 Performance on the VEDAI Dataset:

To further probe the model's capabilities, particularly for the challenging task of small object detection, we extended our evaluation to the VEDAI dataset. This benchmark is characterized by its high proportion of small objects and the use of oriented bounding boxes (OBB), posing a significant test for a detector's precision. As detailed in Table 2, PACGNet achieves a state-of-the-art mAP50 of 82.1% on this dataset. This outstanding result not only places our model at the forefront of performance, surpassing the strong SOTA method  $S_4^6$ -MSTD (81.2%), but also significantly outperforms other competitive models like OST (78.6%) and YOLOFusion (75.9%).

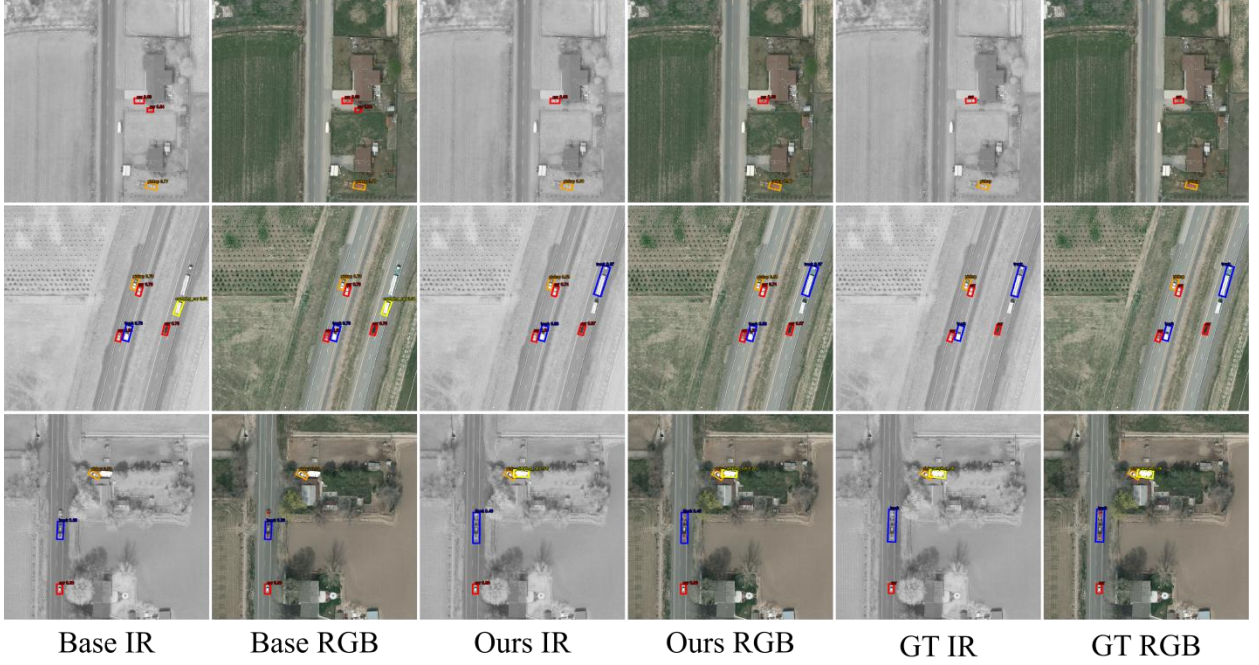


**Figure 4.** Qualitative comparison on the VEDAI dataset. Our PACGNet demonstrates comprehensive improvements over the baseline. It not only reduces false negatives and suppresses false positives/classification errors, but also provides more precise localization for correctly identified targets.

Crucially, PACGNet's superior performance on the VEDAI dataset, which is predominantly composed of small targets, highlights the model's particular strengths in small object detection. This result strongly suggests that our proposed PFMG and SCG modules are highly effective at capturing the fine-grained details and contextual cues necessary to identify small objects in complex aerial scenes. This firmly establishes PACGNet as a small-target-friendly model. A closer look at the per-category performance in Table 2 reveals that PACGNet delivers highly competitive or top-tier results across a majority of classes, including 'truck' (87.1%) and 'tractor' (87.4%), showcasing its robustness within this challenging benchmark.

**Table 3.** Comparison of computational complexity and detection accuracy for the proposed PACGNet and selected state-of-the-art multi-modality detectors.

Detectors	Params.(M)	GFLOPs	mAP50
UA-CMDet[21]	138.7	-	64.0
S <sup>2</sup> A-Net[36]	38.6	93.0	64.8
LF-MD[38]	38.7	77.7	71.8
C <sup>2</sup> Former[22]	101.0	258.3	74.2
MGMF[40]	122.0	-	80.3
PACGNet(our)	<b>5.2</b>	<b>13.2</b>	<b>81.7</b>

Despite the inter-category performance variations on DroneVehicle, the SOTA overall mAP50 scores achieved by PACGNet on both the general-purpose DroneVehicle benchmark (81.7%) and the small-target-focused VEDAI benchmark (82.1%) robustly demonstrate the overall effectiveness and sophistication stemming from the synergistic interplay between our proposed PFMG and SCG modules. This architecture, built upon the strong YOLOv8 foundation, successfully enhances the utilization efficiency of multi-modal information while maintaining computational efficiency (see Table 3), setting a new performance standard in multi-modal detection, especially for scenarios involving small objects. The qualitative results on the VEDAI dataset, shown in Figure 4, further corroborate these findings. The visual comparison highlights PACGNet's comprehensive improvements, showcasing its ability to pr

ovide more precise localization while suppressing false positives and classification errors, which is critical for a small-target-friendly model.

#### 4.4. Ablation Study

To validate the effectiveness and individual contributions of the core components within our proposed PACG Net – namely the Pyramidal Feature-aware Multimodal Gating (PFMG) and Symmetrical Cross-Gating (SCG) modules – a series of ablation experiments were conducted. We established a standard dual-stream YOLOv8 architecture as the baseline and progressively integrated each module. To provide a comprehensive analysis, performance was evaluated on both the VEDAI dataset (mAP(a)) to assess small object detection capabilities and the DroneVehicle dataset (mAP(b)) for general performance. The detailed quantitative results are systematically presented in Table 4.

**Table 4.** Ablation study for PFMG and SCG modules. Checkmarks (✓) denote module inclusion. mAP(a): VEDAI; mAP(b): DroneVehicle. Red marks indicate the best performance.

Method	PFMG	SCG	mAP(a)	mAP(b)	Params.	FLOPs
Baseline			74.1	80.1	4.3M	<b>11.6G</b>
Baseline + PFMG✓			76.7	80.7	4.7M	12.3G
Baseline + SCG	✓		76.6	80.8	4.8M	12.5G
PACGNet(our)	✓	✓	<b>82.1</b>	<b>81.7</b>	<b>5.2M</b>	13.2G

##### 4.4.1. Effectiveness of Individual Components:

Our investigation began by evaluating the impact of incorporating each module in isolation. The baseline model registered an mAP50 of 74.1% on VEDAI and 80.1% on DroneVehicle. As indicated in Table 4:

**Baseline + PFMG:** Adding only the PFMG module improved performance to 76.7% on VEDAI (+2.6% gain) and 80.7% on DroneVehicle (+0.6% gain). This confirms that the PFMG module's hierarchical spatial gating mechanism effectively enhances feature representation, leading to notable improvements, especially in the context of small, hard-to-detect objects.

**Baseline + SCG:** Similarly, integrating only the SCG module elevated performance to 76.6% on VEDAI (+2.5% gain) and 80.8% on DroneVehicle (+0.7% gain). This result substantiates the efficacy of the SCG module's cross-modal gating mechanisms in extracting and leveraging inter-modal complementary cues to boost detection accuracy across both benchmarks.

These initial results clearly demonstrate that both the PFMG and SCG modules are effective components that individually contribute to performance gains, with their impact being particularly pronounced on the small-object-centric VEDAI dataset.

##### 4.4.2. Synergy of Combining PFMG and SCG in PACGNet:

The final stage of our ablation study involved integrating both the PFMG and SCG modules to form the complete PACGNet architecture. This final configuration achieved a state-of-the-art mAP50 of 82.1% on the VEDAI dataset and 81.7% on the DroneVehicle dataset. This represents a total improvement of 8.0% over the baseline on VEDAI and 1.6% on DroneVehicle.

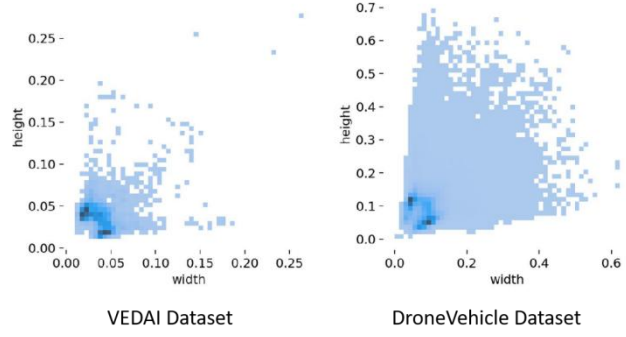


**Figure 5.** Comparison of ground truth bounding box size distributions between the DroneVehicle and VEDAI datasets.

The results reveal a powerful synergy between the PFMG and SCG modules. On the VEDAI dataset, their combined use yields an 8.0% mAP improvement over the baseline, significantly exceeding the sum of their individual gains (+2.6% for PFMG and +2.5% for SCG). This non-additive effect is particularly pronounced on VEDAI due to its high density of small-scale objects (Figure 5). We infer that the two modules play complementary roles in this challenging scenario: the SCG module enriches the features of small targets by fusing cross-modal information, while the PFMG module's top-down gating preserves the fine-grained spatial details crucial for their precise localization. This combination of feature enhancement and detail preservation is the key driver behind PACGN et's superior performance in small object detection.

### 3) Visualization Analysis:

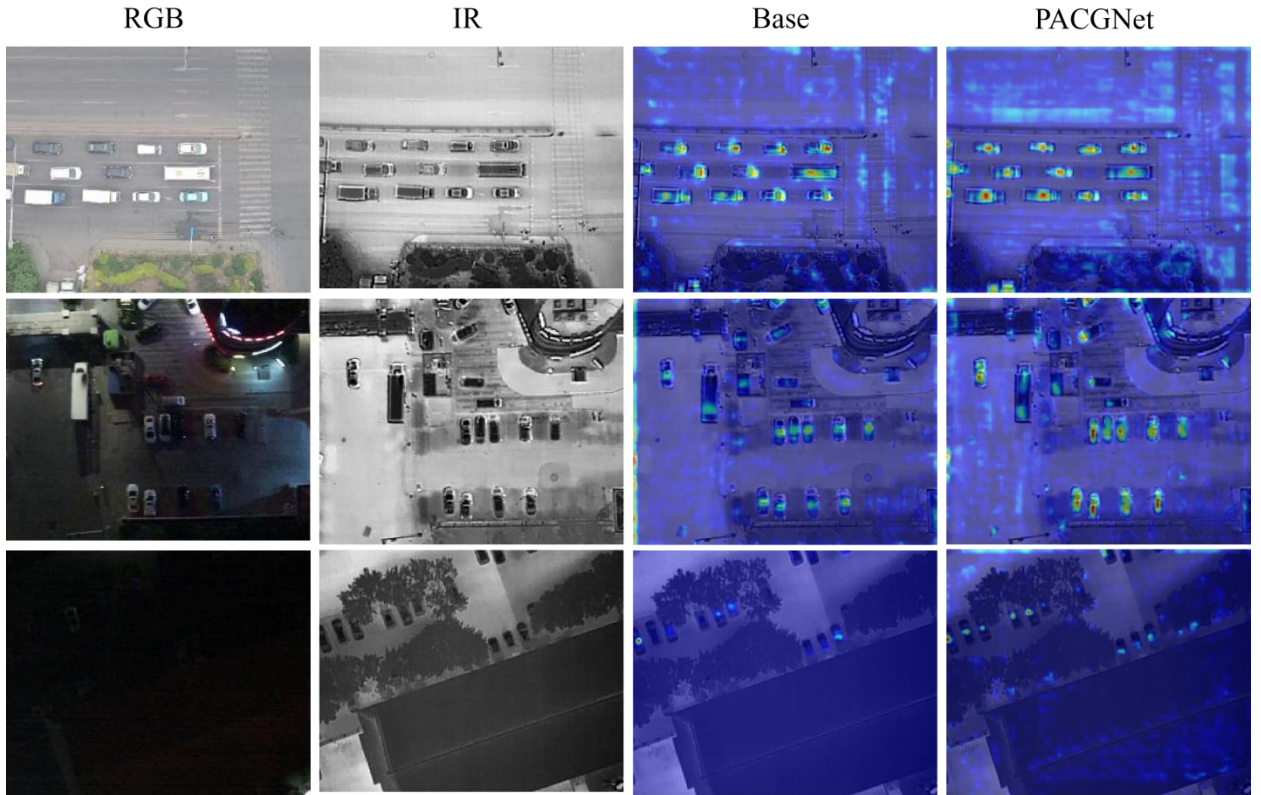


**Figure 6.** Visualization comparing feature activations: Original images, Baseline heatmaps, and PACGNet heatmaps. PACGNet demonstrates enhanced focus encompassing the entire vehicle relative to the Baseline.

To visually substantiate the improvements afforded by our proposed modules, Figure 6 presents comparative feature activation heatmaps between the baseline model and the final PACGNet on identical input imagery. A clear observation is that, relative to the baseline, PACGNet's activation maps exhibit sharper focus on genuine vehicle target regions while simultaneously showing markedly attenuated responses in background areas. This visualization qualitatively confirms the synergistic effect of the SCG and PFMG modules in guiding the network towards learning more discriminative and target-centric fused feature representations.

## 5. Conclusion

In this paper, we introduced PACGNet, a novel Pyramidal Adaptive Cross-Gating Network designed for multimodal object detection in aerial imagery. Our approach distinctively addresses critical challenges in feature-level fusion by completing deep, hierarchical fusion entirely within the backbone, prior to the neck network. To achieve this, we proposed two core modules: the Symmetrical Cross-Gating (SCG) module, which facilitates adaptive "horizontal" feature interaction to selectively exchange complementary information while suppressing cross-modal noise and preserving modality-specific semantics. Complementing this, the Pyramidal Feature-aware Multimodal Gating (PFMG) module rebuilds the feature hierarchy through a progressive gating mechanism that aligns with the backbone's feature extraction flow. By using features from higher-resolution levels to guide the fusion at subsequent, lower-resolution levels, it effectively preserves the fine-grained details crucial for small object detection.

Extensive experiments conducted on the challenging DroneVehicle and VEDAI datasets validate the superiority of our method. PACGNet establishes a new state-of-the-art, demonstrating significant performance gains over existing single-modality and multimodal detectors. The synergistic interplay between the SCG and PFMG modules proves particularly effective for small object detection, a common challenge in aerial scenes. In future work, we will investigate the generalization of our proposed cross-gating and pyramidal fusion principles to other multimodal tasks within the remote sensing field, such as semantic segmentation and change detection.

## REFERENCES

- [1] Person, M., Jensen, M., Smith, A. O., & Gutierrez, H. (2019). Multimodal fusion object detection system for autonomous vehicles. *Journal of Dynamic Systems, Measurement, and Control*, 141(7), 071017.
- [2] Liu, W., Zhang, T., Huang, S., & Li, K. (2022). A hybrid optimization framework for UAV reconnaissance mission planning. *Computers & Industrial Engineering*, 173, 108653.
- [3] Zheng, Z., Zhong, Y., Wang, J., & Ma, A. (2020). Foreground-aware relation network for geospatial object segmentation in high spatial resolution remote sensing imagery. In *Proceedings of the IEEE/CVF conference on computer vision and pattern recognition* (pp. 4096-4105).
- [4] Yao, H., Zhang, Y., Jian, H., Zhang, L., & Cheng, R. (2023). Nighttime pedestrian detection based on Fore-Background contrast learning. *Knowledge-Based Systems*, 275, 110719.
- [5] Zhang, H., Liu, K., Gan, Z., & Zhu, G. N. (2025). UAV-DETR: efficient end-to-end object detection for unmanned aerial vehicle imagery. *arXiv preprint arXiv:2501.01855*.
- [6] Zhang, Y., Zhang, Y., Shi, Z., Fu, R., Liu, D., Zhang, Y., & Du, J. (2023). Enhanced cross-domain dim and small infrared target detection via content-decoupled feature alignment. *IEEE Transactions on Geoscience and Remote Sensing*, 61, 1-16.
- [7] Zhao, Z., Zhang, W., Xiao, Y., Li, C. & Tang, J. (2025). Reflectance-Guided Progressive Feature Alignment Network for All-Day UAV Object Detection. *IEEE Transactions on Geoscience and Remote Sensing*, 63(), 1-15. <https://doi.org/10.1109/TGRS.2025.3574963>
- [8] Zhang, J., Lei, J., Xie, W., Fang, Z., Li, Y., & Du, Q. (2023). SuperYOLO: Super resolution assisted object detection in multimodal remote sensing imagery. *IEEE Transactions on Geoscience and Remote Sensing*, 61, 1-15.
- [9] Dong, W., Zhu, H., Lin, S., Luo, X., Shen, Y., Guo, G., & Zhang, B. (2025). Fusion-mamba for cross-modality object detection. *IEEE Transactions on Multimedia*.
- [10] Geng, M., Zhu, L., Wang, L., Zhang, W., Xiong, R., & Tian, Y. (2024). Event-based visible and infrared fusion via multi-task collaboration. In *Proceedings of the IEEE/CVF Conference on Computer Vision and Pattern Recognition* (pp. 26929-26939).
- [11] Zhang, Q., Wang, W., Liu, Y., Zhou, L., Zhao, H., An, J., & Wang, Z. (2025). Selective Structured State Space for Multispectral-fused Small Target Detection. *arXiv preprint arXiv:2505.14043*.
- [12] Bao, W., Huang, M., Hu, J., & Xiang, X. (2025). Dual dynamic cross-modal interaction network for multimodal remote sensing object detection. *IEEE Transactions on Geoscience and Remote Sensing*.
- [13] Yuan, M., Shi, X., Wang, N., Wang, Y., & Wei, X. (2024). Improving RGB-infrared object detection with cascade alignment-guided transformer. *Information Fusion*, 105, 102246.
- [14] Liu, J., Zhang, S., Wang, S., & Metaxas, D. N. (2016). Multispectral deep neural networks for pedestrian detection. *arXiv preprint arXiv:1611.02644*.
- [15] Solovyev, R., Wang, W., & Gabruseva, T. (2021). Weighted boxes fusion: Ensembling boxes from different object detection models. *Image and Vision Computing*, 107, 104117.
- [16] Li, C., Song, D., Tong, R., & Tang, M. (2018). Multispectral pedestrian detection via simultaneous detection and segmentation. *arXiv preprint arXiv:1808.04818*.
- [17] Wolpert, A., Teutsch, M., Sarfraz, M. S., & Stiefelhagen, R. (2020). Anchor-free small-scale multispectral pedestrian detection. *arXiv preprint arXiv:2008.08418*.
- [18] Qingyun, F., Dapeng, H., & Zhaokui, W. (2021). Cross-modality fusion transformer for multispectral object detection. *arXiv preprint arXiv:2111.00273*.
- [19] Xie, X., Cheng, G., Wang, J., Yao, X., & Han, J. (2021). Oriented R-CNN for object detection. In *Proceedings of the IEEE/CVF international conference on computer vision* (pp. 3520-3529).
- [20] Liu, S., Qi, L., Qin, H., Shi, J., & Jia, J. (2018). Path aggregation network for instance segmentation. In *Proceedings of the IEEE conference on computer vision and pattern recognition* (pp. 8759-8768).
- [21] Sun, Y., Cao, B., Zhu, P., & Hu, Q. (2022). Drone-based RGB-infrared cross-modality vehicle detection via uncertainty-aware learning. *IEEE Transactions on Circuits and Systems for Video Technology*, 32(10), 6700-6713.

[22] Yuan, M., & Wei, X. (2024). C<sup>2</sup>former: Calibrated and complementary transformer for rgb-infrared object detection. *IEEE Transactions on Geoscience and Remote Sensing*, 62, 1-12.

[23] Wang, J., Xu, C., Zhao, C., Gao, L., Wu, J., Yan, Y., ... & Su, N. (2024). Multimodal object detection of UAV remote sensing based on joint representation optimization and specific information enhancement. *IEEE Journal of Selected Topics in Applied Earth Observations and Remote Sensing*, 17, 12364-12373.

[24] Liu, K., Li, T., & Peng, D. (2025). Aerial image object detection based on RGB-Infrared multi-branch progressive fusion. *IEEE Transactions on Geoscience and Remote Sensing*.

[25] Zhang, H., Fromont, E., Lefèvre, S., & Avignon, B. (2021). Guided attentive feature fusion for multispectral pedestrian detection. In *Proceedings of the IEEE/CVF winter conference on applications of computer vision* (pp. 72-80).

[26] Qingyun, F., & Zhaokui, W. (2022). Cross-modality attentive feature fusion for object detection in multispectral remote sensing imagery. *Pattern Recognition*, 130, 108786.

[27] Chen, C., Qi, J., Liu, X., Bin, K., Fu, R., Hu, X., & Zhong, P. (2024). Weakly misalignment-free adaptive feature alignment for uavs-based multimodal object detection. In *Proceedings of the IEEE/CVF Conference on Computer Vision and Pattern Recognition* (pp. 26836-26845).

[28] Ouyang, J., Jin, P., & Wang, Q. (2024). Multimodal feature-guided pre-training for RGB-T perception. *IEEE Journal of Selected Topics in Applied Earth Observations and Remote Sensing*.

[29] Woo, S., Park, J., Lee, J. Y., & Kweon, I. S. (2018). Cbam: Convolutional block attention module. In *Proceedings of the European conference on computer vision (ECCV)* (pp. 3-19).

[30] Wang, Q., Wu, B., Zhu, P., Li, P., Zuo, W., & Hu, Q. (2020). ECA-Net: Efficient channel attention for deep convolutional neural networks. In *Proceedings of the IEEE/CVF conference on computer vision and pattern recognition* (pp. 11534-11542).

[31] Zhang, J., Lei, J., Xie, W., Li, Y., Yang, G., & Jia, X. (2023). Guided hybrid quantization for object detection in remote sensing imagery via one-to-one self-teaching. *IEEE transactions on geoscience and remote sensing*, 61, 1-15.

[32] G. Jocher, A. Chaurasia, & J. Qiu. (2023). Ultralytics YOLOv8. [Online]. Available: <https://github.com/ultralytics/ultralytics>

[33] Tong, Z., Chen, Y., Xu, Z., & Yu, R. (2023). Wise-IoU: bounding box regression loss with dynamic focusing mechanism. *arXiv preprint arXiv:2301.10051*.

[34] Sun, Y., Cao, B., Zhu, P., & Hu, Q. (2022). Drone-based RGB-infrared cross-modality vehicle detection via uncertainty-aware learning. *IEEE Transactions on Circuits and Systems for Video Technology*, 32(10), 6700-6713.

[35] Razakarivony, S., & Jurie, F. (2016). Vehicle detection in aerial imagery: A small target detection benchmark. *Journal of Visual Communication and Image Representation*, 34, 187-203.

[36] Han, J., Ding, J., Li, J., & Xia, G. S. (2021). Align deep features for oriented object detection. *IEEE transactions on geoscience and remote sensing*, 60, 1-11.

[37] Ding, J., Xue, N., Long, Y., Xia, G. S., & Lu, Q. (2019). Learning RoI transformer for oriented object detection in aerial images. In *Proceedings of the IEEE/CVF conference on computer vision and pattern recognition* (pp. 2849-2858).

[38] Sun, X., Yu, Y., & Cheng, Q. (2024). Low-rank multimodal remote sensing object detection with frequency filtering experts. *IEEE Transactions on Geoscience and Remote Sensing*.

[39] He, X., Tang, C., Zou, X., & Zhang, W. (2023, October). Multispectral object detection via cross-modal conflict-aware learning. In *Proceedings of the 31st ACM International Conference on Multimedia* (pp. 1465-1474).

[40] Wang, S., Wang, C., Shi, C., Liu, Y., & Lu, M. (2024). Mask-guided mamba fusion for drone-based visible-infrared vehicle detection. *IEEE Transactions on Geoscience and Remote Sensing*.

[41] Qingyun, F., & Zhaokui, W. (2022). Cross-modality attentive feature fusion for object detection in multispectral remote sensing imagery. *Pattern Recognition*, 130, 108786.

[42] Shen, J., Chen, Y., Liu, Y., Zuo, X., Fan, H., & Yang, W. (2024). ICAFusion: Iterative cross-attention guided feature fusion for multispectral object detection. *Pattern Recognition*, 145, 109913.